Proceedings of the ASME 2010 3rd Joint US-European Fluids Engineering Summer Meeting and 8th International Conference on Nanochannels, Microchannels, and Minichannels
FEDSM-ICNMM2010
August 1-5, 2010, Montreal, Canada

FEDSM-ICNMM2010-30271

THE EFFECT OF SOUND PRESSURE ON THE AEROACOUSTIC SOURCES AROUND TWO DUCTED TANDEM CYLINDERS

Shane Leslie Finnegan*
Craig Meskell
Department of Mechanical and Manufacturing Engineering
Trinity College Dublin
Ireland
Email: finnegsl@tcd.ie

Samir Ziada
Department of Mechanical Engineering
McMaster University
Hamilton, Ontario
Canada

ABSTRACT

An empirical investigation of the spatial distribution of aeroacoustic sources around two tandem cylinders subject to ducted flow and forced transverse acoustic resonance is described. The work builds on a previous investigation by the authors and utilises Howe's theory of aerodynamic sound. The influence of the sound pressure level in the duct on the strength and location of the aeroacoustic sources in the flow was the main focus of the investigation and experiments to resolve the aeroacoustic source distribution were concentrated at a low mainstream flow velocity (before acoustic-Strouhal coincidence), at a medium mainstream flow velocity (just after acoustic-Strouhal coincidence) and at a high mainstream flow velocity (substantially higher than acoustic-Strouhal coincidence). The sound pressure level was found to have a considerable effect on the "lock-in"' range of the cylinders which widened as the sound pressure level increased. A proposed normalisation of the net acoustic energy transfer per spanwise location appears to show good metric for the distribution of the aeroacoustic sources in the flow field. Using this, it was found that the amplitude of the sound pressure had a negligible influence on the aeroacoustic sources in the wake and the gap region for all the tested cases apart from the lowest flow velocity. This particular case showed indications that the aeroacoustic source strength and location could be altered for certain changes in sound pressure level.

*Address all correspondence to this author.

INTRODUCTION

The acoustic resonance of ducted bluff bodies has received much attention in recent years because of its applicability to real engineering systems typical of those found in a gas power plant, for example, packet boilers and heat exchangers. Acoustic resonance of these systems occur when fluctuating pressure disturbances (vortices) shed from the surfaces of the bluff bodies interact with the natural acoustics of the duct. The two tend to feedback into each other and simultaneously enhance each other's regimes. Acoustic resonance typically occurs when the vortex shedding frequency is nearly coincident with the natural acoustic frequency of the duct (acoustic-Strouhal coincidence) and often results in an acute increase in sound pressure throughout the system which is both annoying to plant personnel and may surpass the dynamic head of the system which could be critical in terms of structural liability.

Whilst much work has been completed into investigating acoustic resonance of tube arrays on an experimental and industrial scale by various authors (see for example Ziada et al. [1], Fitzpatrick [2] and Eisinger and Sullivan [3]), the academic torch has also been concentrated on the less complex cylinder configurations, namely two tandem cylinders as they essentially form the core of a tube array. Authors that have concentrated on two tandem cylinders include Mohany and Ziada [4,5], Hall et al. [6], Fitzpatrick [7] and Finnegan et al. [8,9]. Fitzpatrick [7] and Hall et al. [6] have contributed to our understanding of the frequency of the excitation sources and the acoustic field's ability to entrain the vortex shedding frequency whilst Mohany and Ziada [4, 5] and Finnegan et al. [8, 9] have contributed to our understanding of flow-acoustic coupling around the cylinders.

Flow-acoustic coupling around a bluff body in cross-flow is an important and exciting field that accommodates estimations of the generated acoustic power. Identification of the sources surrounding a bluff body could help develop new mitigation techniques for acoustic resonance in industrial heat exchangers. Flow-acoustic coupling utilises the acoustic analogy developed by Howe [10, 11]. A simple expression for the dissipation of sound from an edge, see Eqn 1, determines the acoustic power generated by vorticity in the flow. Howe's integral can be expressed as

$$\Pi = -\rho \int \underline{\omega} \cdot (\underline{U_a} \times \underline{V}) d\Re \tag{1}$$

and is the integral of the triple product between the vorticity vector $\underline{\omega}$, the flow velocity vector $\underline{V}$ and the acoustic particle velocity vector $\underline{U_a}$ where ρ is the mean density of the volume $\Re$. The net acoustic energy is calculated by integrating the time resolved acoustic power over the complete wave cycle. Acoustic energy will be generated if the integral is positive over the whole cycle and absorbed if the integral is negative over the whole cycle.

Finnegan et al. [8, 9] and Mohany and Ziada [5] utilised Eqn. 1 to investigate flow-acoustic coupling around two tandem cylinders, which can have two resonant regimes; namely pre-coincidence acoustic resonance and coincidence acoustic resonance [4]. Pre-coincidence acoustic resonance occurs at high Strouhal numbers where the frequency of the vortex shedding from the cylinders is less than the natural acoustic frequency of the duct whilst coincidence acoustic resonance occurs at lower Strouhal numbers where the frequency of vortex shedding is higher than the natural acoustic frequency of the duct. Numerical simulations completed by Mohany and Ziada [5] provided qualitative evidence that pre-coincidence resonance is driven by shear-layer instability between the cylinders and revealed that coincidence resonance is driven by vortex shedding in the wake. Later, using experimental means rather than numerical simulations, Finnegan et al [8, 9] observed a similar behaviour for a comparable setup but noticed that the wake provided a stronger contribution to pre-coincidence than suggested by Mohany and Ziada [5]. Finnegan et al [8, 9] noted that this discrepancy between the experimental results and the numerical simulations was probably due to differences between the flow and the acoustic fields of both cases. Nonetheless, their results agreed well with Mohany and Ziada [4, 5] and they concluded that pre-coincidence resonance was driven or at least partly driven by a combination of gap shear layer instability and wake vortex shedding.

Whilst the work of Finnegan et al. [8, 9] successfully utilised semi-empirical techniques to quantitatively resolve flow-acoustic coupling around a bluff body subject to cross-flow, their study only investigated forced acoustic resonance and only at one sound pressure level (SPL). That is to say, their experiments could only simulate the interaction mechanisms reported by Mohany and Ziada [4] for one particular SPL and therefore could not comment on its influence on the acoustic source distribution in the duct during resonance, which could be influential [12] . The current paper investigates this effect for the same configuration reported by Finnegan et al. [8, 9], and utilises the same experimental procedures. Therefore it is a direct extension of their previously documented experiments into flow-acoustic coupling around two cylinders and as before, utilises forced acoustic resonance. The main focus is to simulate the influence of the SPL on the pre-coincidence and coincidence acoustic resonance regimes by investigating the spatial distributions and strength of the "locked-in"' acoustic sources around the cylinders. Another goal of the paper is to investigate the influence of the SPL on the acoustic interaction mechanism at acoustic-Strouhal coincidence, which as Mohany and Ziada [13] reported, is non-resonant. Figure 1, which is adapted from their work, shows the aeroacoustic response measured for two tandem cylinders with a similar configuration to the one currently tested. As can be seen, near acoustic-Strouhal coincidence, there is an acute drop in the acoustic pressure, P^*. This means there is no natural, or self-excited acoustic resonance generated by the cylinders at the instant of acoustic-Strouhal coincidence. This paper investigates if changing the SPL in the system has an influence on this and investigates if changing the SPL has any effect on the pre-coincidence and coincidence acoustic resonance regimes.

EXPERIMENTAL SETUP AND TECHNIQUE

Tests were completed in an open loop draw down wind tunnel and utilised air as the working fluid. A schematic of the test section can be seen in Fig. 2 and a detailed description of the geometric dimensions can be found in Finnegan et al. [8, 9]. The tested tandem cylinder configuration had a centre to centre pitch ratio, $P/D = 2.5$, and diameter, $D = 13$mm. Side-branches were employed in the test section because the maximum flow velocity in the tunnel, $V_\infty = 41$m/s, was insufficient to excite the first transverse acoustic mode of the duct when it had an entirely square cross section. Thus, adding the side-branches lowered the natural acoustic frequency of the test section and thereby brought the acoustic "lock-in" range to the capability of the fan. Furthermore, the side-branches concentrated the acoustic energy around the cylinders because their acoustic resonance modes are trapped modes with minimal radiation in the main duct [12]. In this case, the acoustic flux is concentrated between the opening of the branches and the two tandem cylinders are positioned where the acoustic particle velocity is at its maximum. Minimising the radiation losses facilitated the excitation of the lowest resonance mode at various SPL amplitudes by means of loudspeakers which

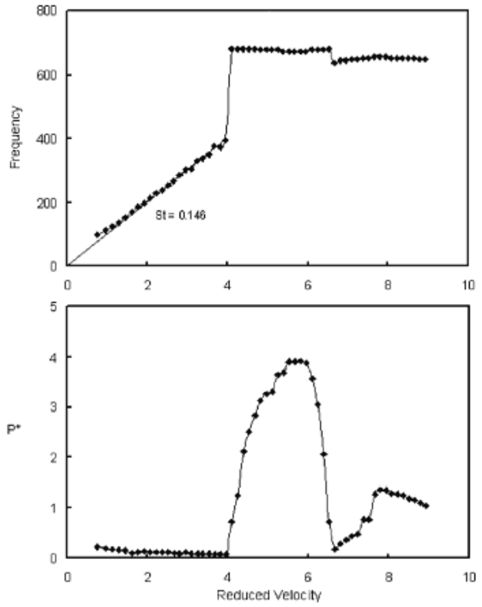

Figure 1. Aeroacoustic characteristics recorded by Mohany and Ziada [13] for natural acoustic resonance of two tandem cylinders.

were attached to the closed ends of the branches and wired 180° out of phase with each other.

Two different flow velocities were selected in order to simulate the pre-coincidence resonance regime and the coincidence resonance regime whilst a third velocity was selected to investigate the case near acoustic-Strouhal coincidence. The three selected flow velocities, expressed in terms of reduced velocity, $U_r = V_\infty/(f_a D)$, were $U_r = 5.9$ (low velocity), $U_r = 6.8$ (medium velocity) and $U_r = 7.7$ (high velocity). If cross referenced with Fig. 1, it is clear to see that the tested flow velocities corresponded to pre-coincidence acoustic resonance, acoustic-Strouhal coincidence (nearly) and coincidence acoustic resonance respectively. Explanation on how these particular velocities were selected is described below. Varying the SPL was achieved by altering the applied voltage to the input of the loudspeakers. With flow in the duct, the acoustic pressure was measured by microphone at each flow velocity for different input voltages. The root mean square of the pressure signal, P_{rms}, was used to determine the SPL in the duct which was then used to estimate the acoustic particle velocity amplitude, $\overline{U_a}$. Assuming plane wave propagation, $\overline{U_a} = P_{rms}/(\rho c)$, where c is the speed of sound in air and $\rho = 1.25\mathrm{kg/m^3}$ is the mean density of air. This value was then used to determine the normalised acoustic velocity, $\overline{U_a}/V_\infty$ which gives an indication of the forcing applied by the speakers with respect to the mainstream flow velocity. Table 1 gives a summary of the tested experimental parameters.

Case	V_∞ (m/s)	U_r	$\overline{U_a}/V_\infty$
Pre coincidence resonance	25.62	5.9	0.07
(Low Velocity)	25.62	5.9	0.09
	25.62	5.9	0.12
Acoustic-Strouhal coincidence	29.28	6.8	0.016
(Medium Velocity)	29.28	6.8	0.03
	29.28	6.8	0.05
Coincidence resonance	32.9	7.7	0.067
(High Velocity)	32.9	7.7	0.075

Table 1. Summary of the experimental parameters.

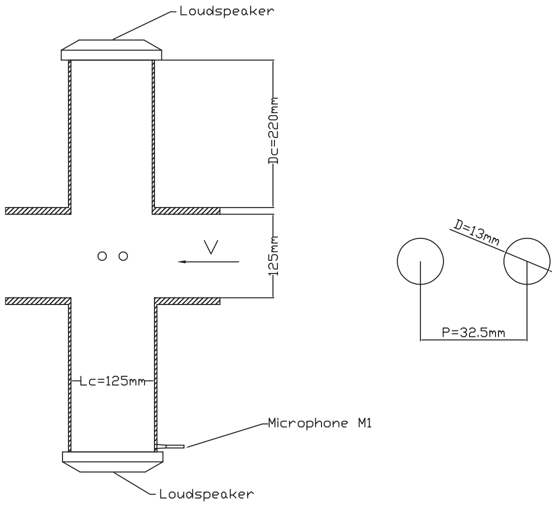

Figure 2. Schematic of the experimental test section.

Figure 3 shows the three components of Howe's integral and the methodology used to resolve these quantities. The unsteady pressure in the test section was recorded using a flush mounted G.R.A.S Type 40BH microphone, M1 as shown in Fig. 2. The measured pressure was then combined with a finite element model of the test section to determine the distribution of the resonant acoustic pressure and acoustic particle velocity. Quantitative characterisation of the hydrodynamic flow field at each selected velocity and SPL amplitude was completed using a low speed LaVision two component, two dimensional particle image velocimetry (PIV) system. 100 images of the unsteady flow field were acquired at every 22.5° of the acoustic wave cycle. Timing of the image acquisition was incorporated in such a way that the order of image phase was acquired at random such that any unknown bias from the measurement was removed. Detailed de-

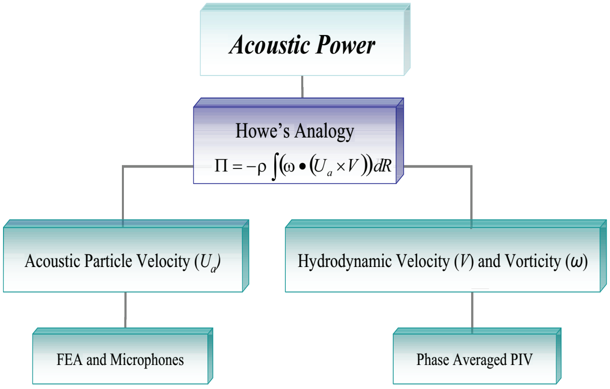

Figure 3. The conceptual approach used to investigate flow-acoustic coupling around the two tandem cylinders.

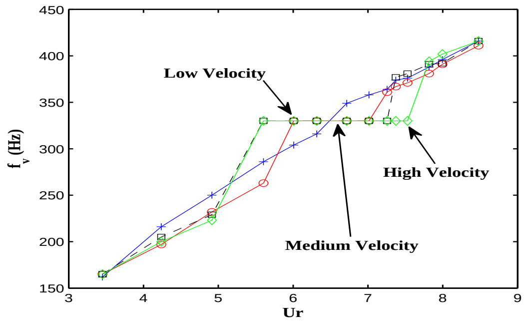

Figure 4. Aeroacoustic characteristics measured by microphone M1 for varying speaker input voltages; $\diamond$ $Voltage = 425$mV, $\square$ $Voltage = 300$mV, $\circ$ $Voltage = 212.5$mV, $+$ No applied voltage.

scriptions of the algorithms used to calculate the acoustic particle velocity and the PIV experimental/processing characteristics can be found in Finnegan et al. [9].

RESULTS

The effect of SPL on the "lock-in"' range

Hall et al. [6] reported that the amplitude of a forced transverse acoustic wave can have substantially influence on the range for which the vortex shedding frequency can be "locked-in"' to the acoustic forcing frequency. It was necessary to investigate this influence for the current set-up in order to determine the appropriate flow velocities at which to perform the PIV measurements. Figure 4 shows a plot of the vortex shedding frequency normalised by the acoustic natural frequency versus reduced velocity for the three tested SPL amplitudes. Spectral analysis of the time signals, measured by microphone M1, as shown in Fig. 2, was used to determine if the flow at a particular velocity was "locked-in"' to the acoustic field. As can be seen, increasing input voltage to the loudspeakers and hence, the SPL increases the width of the "lock-in"' range both before and after acoustic-Strouhal coincidence. That is to say that increasing the SPL promotes a larger frequency shift away from the natural Strouhal frequency of vortex shedding. These findings agree well with those of Hall et al. [6]. One observation that can be made from Fig. 4 is that increasing the SPL from high to very high levels only increases the width of the "lock-in"' range in the coincidence resonance regime and not the pre-coincidence resonance regime. This is likely due to the hysterises effect which often appears at the high end of the "lock-in"' range of self-excited acoustic resonances.

Also shown on the plot is the normalised vortex shedding frequency versus reduced velocity for the case of no applied sound. As can be seen, acoustic "lock-in"' is not self-initiated and the vortex shedding frequency increases linearly with flow velocity. The recorded Strouhal number of vortex shedding based on the diameter of the cylinders, $S_t = 0.15$ is in good agreement with the experiments of Mohany and Ziada [13]. As mentioned, Fig. 4 was also used to determine the flow velocities at which to perform the PIV measurements. Because the effect of the SPL amplitude on the spatial distribution of the acoustic sources was the focus of the study, a selected flow velocity needed to be "locked-in"' for all three sound pressure levels. Figure 4 shows the three velocities tested, which include cases under pre-coincidence resonance, coincidence resonance and a third velocity just after acoustic-Strouhal as discussed above. Based on the Strouhal number, acoustic-Strouhal coincidence occurs at $U_r = 6.6$. Using this, the ratio of the acoustic natural frequency to the vortex shedding frequency, f_a/f_v, for the low velocity case (pre-coincidence resonance) was $f_a/f_v = 1.12$ whilst for the high velocity case (coincidence resonance) was $f_v/f_v = 0.86$. For the medium velocity case (near acoustic-Strouhal coincidence) $f_a/f_v = 0.97$. From here on, the terms low velocity, medium velocity and high velocity and the values for the frequency ratio will be interchanged with each other to describe a particular case. The flow velocity in the duct was controlled using a slider plate at the exhaust of the fan. It should be noted that for the results presented in Fig. 4, the fan settings were randomised which means that the order of the pressure measurements taken by M1 was also randomised. This was done to remove any hysterises and unknown bias from the system.

Acoustic particle velocity (U_a)

The finite element package ANSYS was used to perform modal analysis of a quiescent flow field in the test section and obtain the resonant acoustic pressure distribution (i.e. mode shape). Equation 2 was used to solve the time dependent acoustic particle velocity in the test section. This equation is an expanded version of the Euler equation where P_{FEA} denotes the pressure solved from the modal analysis, ρ represents the mean density of

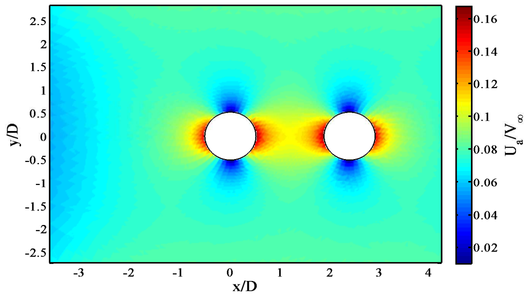

Figure 5. Contours of the acoustic particle velocity normalised by the mainstream velocity, $f_a/f_v = 1.12$, $U_a/V_\infty = 0.12$, $\phi = 180°$.

air and f_a is the resonant acoustic frequency measured by M1. Figure 5 shows the contours of the acoustic particle velocity distribution within the PIV area of interest at phase, $\phi = 180°$ in the acoustic cycle. The phase angle, ϕ refers to the phase of the acoustic pressure measured by M1. The contours are normalised by the mainstream velocity corresponding to $f_a/f_v = 1.12$ and a dimensionless acoustic amplitude of $\overline{U_a}/V_\infty = 0.12$.

$$U_a(x,y,t) = \frac{P_{rms}}{2\pi f_a \rho} cos(2\pi f_a t) \cdot \nabla P_{FEA} \tag{2}$$

The boundary conditions applied to the model were zero acoustic pressure at the inlet and outlet of the test section, making it a Dirichlet boundary-value problem [14]. This boundary condition was selected in order to simulate an open ended duct which facilitated the extraction of the β-mode [15], where the pressure decays exponentially along the length of the duct. Also, the walls where assumed to be an ideal rigid acoustic medium and the test section was modelled in 3D to account for any effects caused by the circular co-axial side branches. The frequency of the acoustic particle velocity solved by the model was 301Hz. The natural frequency measured by M1 on the day of testing was 330Hz, which is 9.6% higher than the numerically computed value. This variation has been attributed to differences in the geometry between the test section and the model, the presence of the loudspeakers at the closed ends of the side-branches (which were not modeled) and discrepancies in the true speed of sound between the model and the test facilities.

Particle image velocimetry (PIV)

Contours of the phase averaged velocity and vorticity for the three flow velocities tested at a phase angle of $\phi = 45°$ in the acoustic pressure wave cycle are shown in Fig. 6. The top row shows velocity contours overlayed with streamlines whilst the bottom row shows the out of plane vorticity. It shows the distribution of the vortices at the same point in the acoustic wave cycle for the three different flow velocities and highlights the differences in the "locked-in"' flow structures. In the bottom row of the figure, red contours represents positive vorticity whilst blue contours represents negative vorticity.

As can be seen, alternate Karman vortex shedding occurs in both the gap and wake regions for both low and medium velocities. Vortices emanating from the separation point on the upstream cylinder roll up and impinge on the downstream cylinder before shedding again into the wake. As the flow velocity increases, the convection speed of the vortices also change and one would expect the structure of the propagating vortices to change as well. This is evident at high velocity, where the vortices in the gap region are elongated compared to the other two cases. However if the low and medium cases are compared, the difference between the flow structures seems to be negligible.

Fluid-acoustic coupling - Acoustic power

The unsteady vorticity in the shear layers, the variation of the velocity across the duct and the fluctuating transverse acoustic wave imposed by the loudspeakers can be coupled together using Howe's theory of aerodynamic sound, see Eqn. 1, in order to determine the aeroacoustic sources in the duct. Time-resolved or phase-averaged acoustic power maps for the three tested velocities are plotted in Fig. 7 for $\phi = 180°, 225°, 270°, 315°$ and $0°$ (from top to bottom). The images in the first and last rows ($\phi = 180°$ and $0°$) correspond to the maximum negative and maximum positive acoustic particle velocity respectively which means the maximum amount of acoustic power is generated (and absorbed) at these phases. In the second row ($\phi = 225°$) at low and medium velocities, vortices just shed from the top side of the upstream cylinders are absorbing energy. However at the same time, a vortex shed from the bottom edge of the upstream cylinder is about to impinge onto the downstream cylinder and is generating energy. Because the vortex is generating acoustic power, it has a positive contribution on the acoustic field. At $\phi = 225°$ there is negligible generation (or absorption) of acoustic power in the wake region at low and medium velocities, however at high velocity there is a long source located here generating acoustic power in this region. This difference in the source/sink locations at the same phase in the acoustic cycle highlights the change in flow structure that occurs between pre-coincidence resonance and coincidence resonance. In the third row, $\phi = 270°$, the acoustic particle velocity is zero and so there is no acoustic power being generated. This means that at $\phi = 270°$, there is no net contribution to the acoustic energy in the system. In the fourth and fifth rows, it can be seen that acoustic power generation has switched polarity and the shear layers shed from the top of the cylinders are now generating power whilst shear layers shed from the bottom of the cylinders are now absorbing power. This is because U_a has switched directions and is positive after passing through zero at $\phi = 270°$.

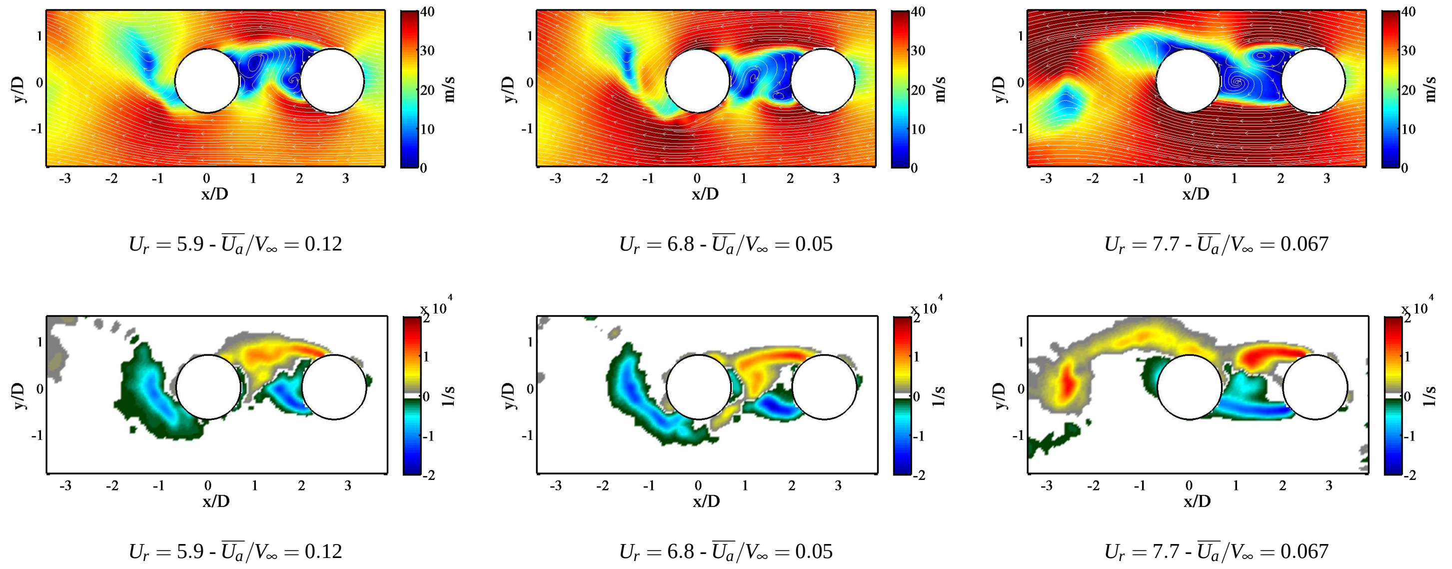

Figure 6. Contours of the “locked-in”' hydrodynamic flow field characteristics for the three tested velocities at the same phase in the acoustic wave cycle, $\phi = 45°$. Velocity - Top row. Vorticity - Bottom row.

Fluid-acoustic coupling - Acoustic energy

The total net acoustic energy generated over the whole cycle can be found by integrating Eqn.1. Figure 8 shows the spatial distributions of the net acoustic energy for all the tested SPL amplitudes at low and medium flow velocities. As can be seen the sources and sinks are symmetric about the centreline of the cylinders which is obviously due to the periodicity of Von-Karman vortex shedding. In the gap region between the cylinders for $f_a/f_v = 1.12$, intense acoustic sources lie in the outer shear layers, hugging two very intense sinks located in the inner shear layers. As the scale suggests, the most intense sources are located in the middle of the gap which agrees well with the previous experiments completed by the authors and with the simulations of Mohany and Ziada [5]. At $f_a/f_v = 0.97$, the structures of the aeroacoustic sources are quite similar to those at low velocity. The one noticeable difference between the low and medium velocities is the existence of two sinks hugging the two sources in the gap region, which in turn are hugging a sink in the region just behind the upstream cylinder. In terms of the wake, the distribution of the aeroacoustic sources are nearly identical. A source can be seen absorbing acoustic energy all around the downstream cylinder which is followed by a cluster of sources generating acoustic energy about 2.5 diameters downstream of the cylinders. What is interesting is that the distribution of the sources for both flow velocities do not change appreciably as the SPL amplitude is increased, in fact, doubling the sound pressure seems to have little to no effect on the distribution of the aeroacoustic sources in neither the gap region nor the wake.

Figure 9 shows the spatial distributions of the net acoustic energy at the two tested SPL amplitudes for the $f_a/f_v = 0.86$ case. The differences in the structures of the net acoustic energy between the low/medium velocities and high velocity are clear to see. Here, strong aeroacoustic sources in the outer shear layers hug two strong sinks. The sources completely engulf the outer shear layer as well as the downstream cylinder and the near wake. Increasing $U_a/V_\infty = 0.067$ to $U_a/V_\infty = 0.075$ seems to also have a negligible effect on the spatial distribution of the aeroacoustic sources. As with the low flow velocity, the distribution of the aeroacoustic sources and sinks at high flow velocity agree well with the previous work of Finnegan et al. [8,9] and Mohany and Ziada [5], strengthening the supposition that pre-coincidence acoustic resonance is driven by a combination of shear layer instability and vortex shedding in the wake whilst coincidence acoustic resonance seems to be driven by vortex shedding in the wake.

DISCUSSION

The influence of SPL on the aeroacoustic sources

Spatial distributions of the phase averaged acoustic power and net acoustic energy around two tandem cylinders subject to ducted flow have been determined for three different sound pressure levels at reduced velocities of $U_r = 5.9, 6.8$ and 7.7. These reduced velocities correspond to pre-coincidence acoustic resonance, acoustic-Strouhal coincidence (nearly) and coincidence acoustic resonance respectively. Whilst Fig. 7, Fig. 8 and Fig. 9 give good qualitative indications of the influence of SPL on the aeroacoustic sources around the cylinders, a more quantitative

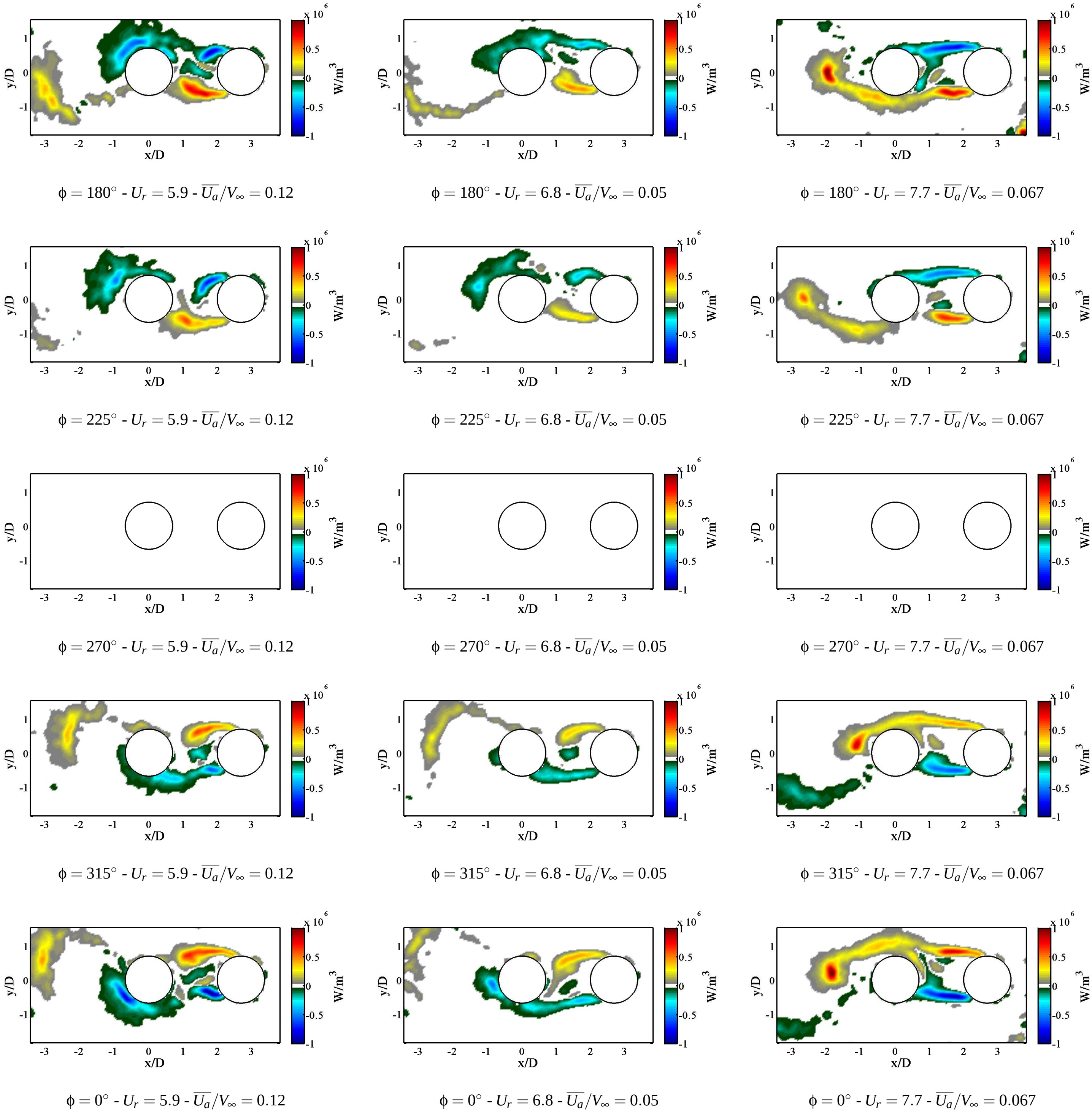

Figure 7. Contours of the resonant acoustic power at the three tested flow velocities.

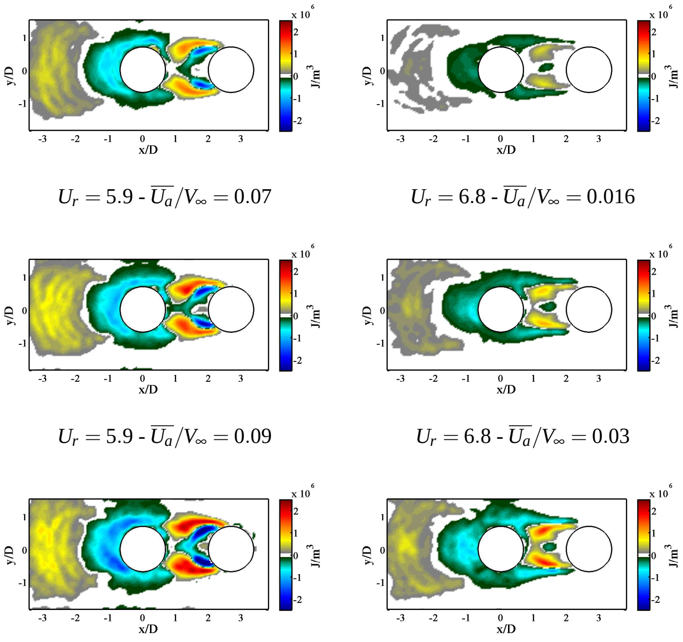

$U_r = 5.9$ - $\overline{U_a}/V_\infty = 0.07$ $U_r = 6.8$ - $\overline{U_a}/V_\infty = 0.016$

$U_r = 5.9$ - $\overline{U_a}/V_\infty = 0.09$ $U_r = 6.8$ - $\overline{U_a}/V_\infty = 0.03$

$U_r = 5.9$ - $\overline{U_a}/V_\infty = 0.12$ $U_r = 6.8$ - $\overline{U_a}/V_\infty = 0.05$

Figure 8. Contours of the resonant net acoustic energy. Left - low velocity ($f_a/f_v = 1.12$), Right - medium flow velocity ($f_a/f_v = 0.97$).

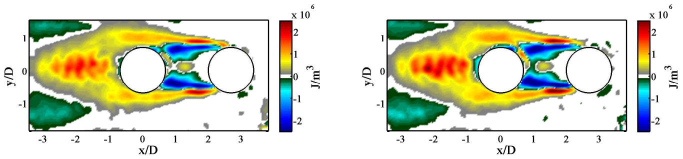

$U_r = 7.7$ - $\overline{U_a}/V_\infty = 0.067$ $U_r = 7.7$ - $\overline{U_a}/V_\infty = 0.075$

Figure 9. Contours of the resonant net acoustic energy high velocity ($f_a/f_v = 0.86$).

approach is desirable. Figure 10 shows the total acoustic energy per spanwise location, E (J/m^2), at low flow velocity for the three tested SPL amplitudes. From this plot, it is possible to locate the spanwise locations of the net acoustic sources and determine their strength relative to each other. Clearly, at low velocity, net acoustic sources tend to form in the gap region between the cylinders and in the wake of the two cylinders roughly 2.5 diameters downstream.

Varying the SPL simply acts as a scaling factor in Eqn. 1 because the acoustic particle velocity is proportional to the SPL. In order to properly observe the effect of the SPL amplitude, it should be taken out of consideration. A dimensional analysis of the system, revealed that the energy per spanwise location, E, can be normalised by the product of acoustic pressure measured by microphone M1 during a test and the cylinder diameter, that

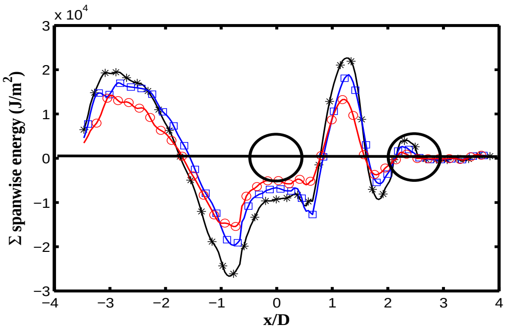

Figure 10. Net acoustic energy transfer per spanwise location at low velocity, $U_r = 5.9$; $*\ \overline{U_a}/V_\infty = 0.12$, $\square\ \overline{U_a}/V_\infty = 0.09$, $\circ\ \overline{U_a}/V_\infty = 0.07$.

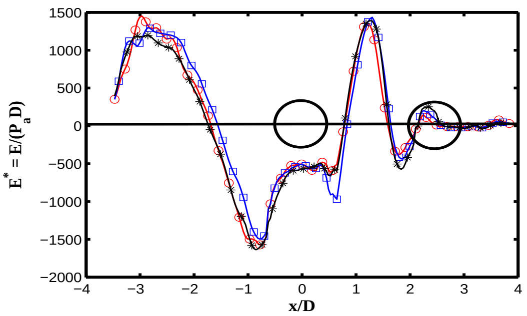

Figure 11. Normalised net acoustic energy transfer per spanwise (E^*) at low velocity, $U_r = 5.9$; $*\ \overline{U_a}/V_\infty = 0.12$, $\square\ \overline{U_a}/V_\infty = 0.09$, $\circ\ \overline{U_a}/V_\infty = 0.07$.

is:

$$E^* = \frac{E}{P_{rms}D} \tag{3}$$

By normalising the total energy per spanwise location using Eqn. 3, the scatter in the data for different SPL amplitudes for pre-coincidence resonance ($f_a/f_v = 1.12$) is greatly reduced as shown in Fig. 11. As this normalisation causes the curves of the three SPL amplitudes to collapse, it provides a good metric for the aeroacoustic source distribution in the flow field at low velocity. Increasing the normalised acoustic velocity from $\overline{U_a}/V_\infty = 0.07$ to $\overline{U_a}/V_\infty = 0.09$ seems to slightly increase the strength of the sources in the gap region whilst encouraging a small shift towards the upstream cylinder yet has a negligible effect on the sources in the wake. Changing the normalised acoustic velocity from $\overline{U_a}/V_\infty = 0.09$ to $\overline{U_a}/V_\infty = 0.12$ does not have the same effect at this velocity.

Figure 12 and Fig. 13 show the normalised acoustic energy per spanwise location calculated using Eqn. 3 for the all

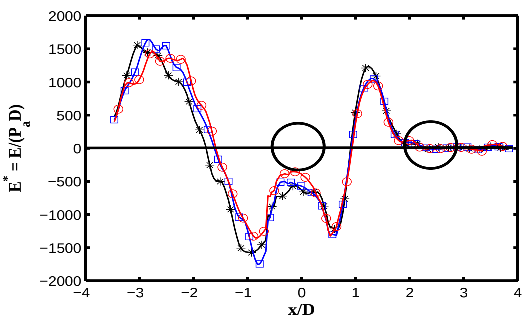

Figure 12. Normalised net acoustic energy transfer per spanwise (E^*) at medium velocity, $U_r = 6.8$; $* \, \overline{U_a}/V_\infty = 0.05$, $\square \, \overline{U_a}/V_\infty = 0.03$, $\circ \, \overline{U_a}/V_\infty = 0.016$.

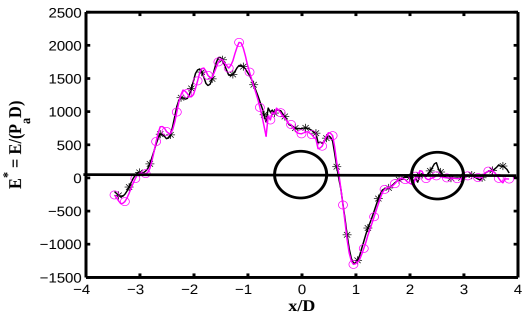

Figure 13. Normalised net acoustic energy transfer per spanwise (E^*) at high velocity, $U_r = 7.7$; $* \, \overline{U_a}/V_\infty = 0.067$, $\circ \, \overline{U_a}/V_\infty = 0.075$.

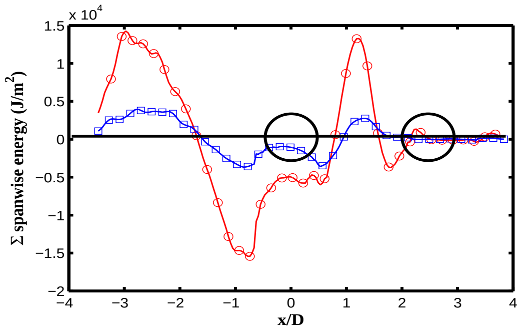

Figure 14. Comparison of the net acoustic energy transfer per spanwise location at the same loudspeaker input voltage. $\circ \, f_a/f_v = 1.12$ ($\overline{U_a}/V_\infty = 0.07$), $\square \, f_a/f_v = 0.97$ ($\overline{U_a}/V_\infty = 0.016$).

the tested SPL amplitudes for medium and high velocities respectively. As can be seen, at medium flow velocity changing $\overline{U_a}/V_\infty = 0.016$ to $\overline{U_a}/V_\infty = 0.03$ has an unnoticeable effect on the source distribution across the system whilst changing from $\overline{U_a}/V_\infty = 0.03$ to $\overline{U_a}/V_\infty = 0.05$ results in a strengthening of the net source in the gap region only. At high flow velocity, varying $\overline{U_a}/V_\infty = 0.067$ to $\overline{U_a}/V_\infty = 0.075$ has virtually no effect on the sources.

It seems that for the three tested flow velocities, increasing the sound pressure level in the duct has relatively little influence on neither the location nor source strength of the aeroacoustic sources. Any influence on the vortex formation and hence the aeroacoustic source that does exist, certainly does not compare to that reported by Ziada [12] for a co-axial side-branch resonator. It should be noted however that the range of excitation used by Ziada [12] (5% to 50% of the mean velocity) was much wider than that used in the present experiments.

The work of Finnegan et al. [8, 9] and Mohany and Ziada [4, 5] have highlighted the differences in the structure of the aeroacoustic sources between pre-coincidence and coincidence acoustic resonance and the current results support their findings. Mohany and Ziada [13] observed that for two tandem cylinders with a similar configuration, the acoustic resonance mechanism was non-existent at acoustic-Strouhal coincidence, that is, the system was not resonating. However, as can be clearly seen from Fig. 8 and Fig. 12, a distribution of sources does exist for this case ($U_r = 6.8$). This is due to the fact that the experiments of Mohany and Ziada [13] exhibited natural acoustic resonance and not forced acoustic resonance. As the resonance exhibited here is forced, the loudspeakers will always supply acoustic energy to the flow regardless of its mainstream velocity. Thus, aeroacoustic sources and sinks will always form in this system regardless of whether it is able to self-sustain the acoustic resonance or not. Figure 14 plots the net acoustic energy transfer per spanwise location for the $f_a/f_v = 1.12$ and $f_a/f_v = 0.97$ cases. Each case corresponds to the SPL of the lowest loudspeaker input voltage. As can be seen, the strength of the acoustic sources and sinks are much smaller for the $f_a/f_v = 0.97$ case compared to the $f_a/f_v = 1.12$ case. Table 2 lists the SPL measured by M1 during a test for a given input voltage. As can be seen the SPL recorded by the microphone at acoustic-Strouhal coincidence is the lowest of all the cases for a given input voltage. Comparing Fig. 14 and Tab. 2 with Fig. 1 explains why the sources and sinks for the near coincidence case are substantially weaker than those observed for the other two cases when the same level of excitation is supplied by the loudspeakers.

CONCLUSIONS

An investigation into the effect of the sound pressure level on the acoustic “lock-in”’ phenomenon and the aeroacoustic source characterisation for a pair of two tandem cylinders has been presented, building on previous work completed by the authors. Tests were performed by varying the mainstream flow velocity and sound pressure level in the duct. The velocities were selected to coincide with the well documented pre-coincidence acoustic resonance and coincidence acoustic resonance regimes and the

U_r	Voltage (mV)	SPL_{M1} (Pa)
5.9	200	768
	300	1030
	425	1276
6.8	200	212
	300	386
	425	628
7.7	425	947
	525	1051

Table 2. List of the SPL for a given loudspeaker input voltage measured by microphone M1 during a PIV test.

sound pressure levels were selected so that the flow field was “locked-in”’ to the resonant acoustic field in all tested cases. The sound pressure level was found to have a considerable effect on the “lock-in”’ range of the cylinders. Investigation of the vortex shedding frequency indicated that increasing the sound pressure level widened the range of flow velocities at which the vortices could be entrained by the acoustic particle velocity. In terms of the flow-acoustic coupling, the distribution of the aeroacoustic sources around the cylinders were found to be in good agreement with the authors’ previous findings and with those found in literature. As the focus of the investigation was to study the effect of sound pressure level, a normalisation of the net acoustic energy transfer per spanwise location, by the product of the acoustic pressure and the cylinder diameter was proposed. This normalisation caused the data to collapse and provided a good metric for the distribution of the aeroacoustic sources in the flow field at the tested velocities. It was found that changing the amplitude of the sound pressure level had a negligible effect on neither the strength nor the location of the aeroacoustic sources in the wake of the cylinders for the tested velocities. Furthermore, it was also found that changing the sound pressure amplitude had relatively little influence on the source location and strength in the gap shear layer region between the cylinders except for the lowest tested velocity which indicated a slight increase in strength and a small shift upstream, but only between the lowest and the middle tested SPL amplitudes. Of the three tested velocities, one occurred just after acoustic-Strouhal coincidence. This case exhibited a slight acoustic resonance that was sustained by the loudspeaker at the end of the side branch. As the loudspeaker forced acoustic energy into the system this phenomenon is not expected to occur for naturally induced acoustic resonance at this flow velocity.

ACKNOWLEDGMENT

The authors acknowledge funding from the Irish Research Council for Science, Engineering and Technology (IRCSET).

REFERENCES

[1] Ziada, S., Oengoren, A., and Buhlmann, E. T., 1989. “On acoustical resonance in tube arrays part ii: Damping criteria”. *Journal of Fluids and Structures*, **3**(3), pp. 315–324.

[2] Fitzpatrick, J. A., 1985. “The prediction of flow-induced noise in heat exchanger tube arrays”. *Journal of Sound and Vibration*, **99**(3), pp. 425–435.

[3] Eisinger, F. L., and Sullivan, R. E., 2007. “Acoustic resonance in a package boiler and its solution - a case study”. *Journal of Pressure Vessel Technology*, **129**, pp. 759–762.

[4] Mohany, A., and Ziada, S., 2005. “Flow-excited acoustic resonance of two tandem cylinders in cross-flow”. *Journal of Fluids and Structures*, **21**(1), pp. 103–119.

[5] Mohany, A., and Ziada, S., 2009. “Numerical simulation of the flow-sound interaction mechanisms of a sinlge and two-tandem cylinders in cross-flow”. *Journal of Pressure Vessel Technology*, **131**(3).

[6] Hall, J. W., Ziada, S., and Weaver, D. S., 2003. “Vortex-shedding from single and tandem cylinders in the presence of applied sound”. *Journal of Fluids and Structures*, **18**(6), pp. 741–758.

[7] Fitzpatrick, J. A., 2003. “Flow/acoustic interactions of two cylinders in cross-flow”. *Journal of Fluids and Structures*, **17**(1), pp. 97–113.

[8] Finnegan, S. L., Meskell, C., and Ziada, S., 2009. “Experimental investigation of the aeroacoustic sources in a tandem cylinder configuration”. In 2009 ASME Pressure Vessels and Piping Division Conference.

[9] Finnegan, S. L., Meskell, C., and Ziada, S., (Under Review). “Experimental investigation of the acoustic power around two tandem cylinders.”. *Journal of Pressure Vessel Technology*.

[10] Howe, M. S., 1975. “Contributions to theory of aerodynamic sound, with application to excess jet noise and theory of flute”. *Journal of Fluid Mechanics*, **71**(4), pp. 625–673.

[11] Howe, M. S., 1980. “The dissipation of sound at an edge”. *Journal of Sound and Vibration*, **70**(3), pp. 407–411.

[12] Ziada, S., 1994. “A flow visualization study of flow-acoustic coupling at the mouth of a resonant side-branch”. *Journal of Fluids and Structures*, **8**(4), pp. 391–416.

[13] Mohany, A., and Ziada, S., 2009. “A parametric study of the resonance mechanisms of two tandem cylinders in cross-flow”. *Journal of Pressure Vessel Technology*, **131**(2).

[14] Hourigan, K., Welsh, M. C., Thompson, M. C., and Stokes, A. N., 1990. “Aerodynamic sources of acoustic resonance in a duct with baffles”. *Journal of Fluids and Structures*, **4**(4), pp. 345–370.

[15] Parker, R., 1967. "Resonance effects in wake shedding from parallel plates: Calculation of resonant frequencies". *Journal of Sound and Vibration*, **5**(2), pp. 330–343.